

RSC Advances



This is an *Accepted Manuscript*, which has been through the Royal Society of Chemistry peer review process and has been accepted for publication.

Accepted Manuscripts are published online shortly after acceptance, before technical editing, formatting and proof reading. Using this free service, authors can make their results available to the community, in citable form, before we publish the edited article. This *Accepted Manuscript* will be replaced by the edited, formatted and paginated article as soon as this is available.

You can find more information about *Accepted Manuscripts* in the [Information for Authors](#).

Please note that technical editing may introduce minor changes to the text and/or graphics, which may alter content. The journal's standard [Terms & Conditions](#) and the [Ethical guidelines](#) still apply. In no event shall the Royal Society of Chemistry be held responsible for any errors or omissions in this *Accepted Manuscript* or any consequences arising from the use of any information it contains.

Manuscript Submitted for Publication in Rsc Advances

Spherical V-MCM-48: The Synthesis, Characterization and
Catalytic Performance in Styrene Oxidation

Haiqing Wang,^a Wang Qian,^a Jin Chen,^a Yong Wu,^{*b} Xiaoying Xu,^a Jun Wang,^a Yan Kong^{*a}

(1. State Key Laboratory of Materials-Oriented Chemical Engineering, Nanjing University of Technology, Nanjing 210009, China;

2. Institute of Chemistry and Environmental Science, Nanjing Normal University, Nanjing, 210097, China)

*: Corresponding Author

Email: kongy36@njtech.edu.cn

Tel: 86-25-83587860

Fax: 86-25-83587860

+: Co-corresponding Author

Email: wuyongnju@gmail.com

Abstract

A series of spherical vanadium-containing mesoporous V-MCM-48 catalysts with different V/Si atomic ratios were synthesized by direct hydrothermal method. The structure and morphology of the samples and the states of vanadium in the materials were systematically characterized by XRD, N₂ physisorption, FE-SEM, HRTEM, ICP, UV-vis, ⁵¹V MAS-NMR, ESR and XPS. The possible formation mechanism of spherical V-MCM-48 was proposed based on Stöber process. Meanwhile, the catalytic activities of the samples were evaluated in the oxidation of styrene to benzaldehyde using H₂O₂ as oxidant. The results show that the V-MCM-48 samples have regularly spherical morphology, homogeneous dispersion and highly ordered cubic mesostructure. Characterization results about the coordination states of vanadium species demonstrated that most of vanadium existed as tetracoordinated V⁴⁺ species in silicate framework and small amount of vanadium as isolated V⁵⁺ species on surface. The prepared spherical V-MCM-48 exhibits much higher catalytic activity in the catalytic conversion of styrene to benzaldehyde. Spherical morphology contributes significantly to the improved catalytic performance of materials. V⁵⁺ species on the surface and/or produced from the oxidation of some V⁴⁺ in the framework act as active sites. Furthermore, the reaction parameters such as vanadium content in V-MCM-48, molar ratio of H₂O₂/styrene, temperature, time and solvents were optimized.

Keywords: MCM-48, Vanadium, Spherical Morphology, Styrene Oxidation.

1. Introduction

Since the researchers at Mobil Research and Development Corporation reported the M41S family,¹ many efforts have been devoted to the synthesis and applications of mesoporous molecular sieves in catalysis,² sorption,^{3,4} drug delivery⁵, biosensor⁶ and so on over the last few decades due to their ordered pore arrangement, narrow pore-size distribution, high specific surface area and thermal stability.

MCM-41 and MCM-48 are two typical members in the well-known M41S family. Compared with the 1D (one-dimensional) pore system of MCM-41, the 3D (three-dimensional) cubic pore network of MCM-48 is recognized as a more promising system with respect to catalytic applications,⁷⁻⁹ because it is not only more favorable to the mass transfer in heterogeneous catalysis, but also more resistant to pore blocking.¹⁰

It is well known that the morphology and the pore structure of supports play very important role in determining both the diffusion of reactants and products in heterogeneous catalysis.¹⁰⁻¹⁵ However, many current studies have focused on the synthesis of MCM-41 with different morphologies with less attention on MCM-48.¹⁶ The synthesis of high-quality MCM-48 with special morphology remains difficult, since it can only be produced in delicate experimental conditions. Minor change in experimental conditions including pH, temperature, aging time or concentration of template may lead to the absence of cubic mesoporous structure.^{10, 17}

Due to the lack of catalytic sites for pure mesoporous silicate materials, the incorporation of transition metals,^{7, 18-24} such as Ti, Mn, Fe, Cu, V, etc. into the framework of M41S has been widely examined. The doping of transition metals can modify the surface acidity/basicity and the redox property of the mesoporous molecular sieves, and

consequently improve their catalytic activity. There are many reports concerning the guest-incorporation into mesoporous silicate matrix including the direct hydrothermal (DHT) method,^{25, 26} the wet impregnation method,²⁷ the grafting method,²⁸ the template ion-exchange (TIE) method⁷ and so on. Especially, the DHT method is considered to be advantageous because of its simplicity of process and higher efficiency in introducing heteroatoms into silicate framework, while other methods either produce more crystalline metal oxide or aggregated metal species outside the framework, which result in easy leaching of active sites in the liquid phase reactions.^{27, 29, 30} However, the heteroatom-doped mesoporous silica prepared via DHT method often exhibit poor morphologies.^{7, 29} The synthesis of mesoporous silicate with both heteroatom doping and regular morphology has to be prepared under optimal conditions. Some synthesis parameters should be controlled precisely for the simultaneous hydrolyzation of heteroatom and silicon species, which ensured the heteroatoms in the framework.^{7, 20, 25, 31} Thus, the synthesis of mesoporous silicate with heteroatoms in the framework and special morphology is full of challenge, especially in the case of MCM-48.

Vanadium-modified mesoporous molecular sieves exhibit high catalytic activity in many reactions, especially in the oxidation of aromatics,^{13, 17, 32, 33} such as benzene, phenol, styrene, etc. In this study, V-MCM-48 catalysts with regular spherical morphology and different vanadium content were synthesized by DHT method and characterized by various techniques. The catalytic performances of produced catalysts were systematically studied in the oxidation of styrene, which is of considerable commercial and academic interest for the synthesis of important products such as styrene epoxide, benzaldehyde and phenylacetaldehyde.^{7, 34} The possible mechanism for the formation of spherical

V-MCM-48 as well as the catalytic process was further discussed.

2. Experimental section

Materials

Surfactant: Cetyltrimethylammonium bromide (CTAB, 99%) was purchased from J&K Chemical Ltd. Tetraethylorthosilicate (TEOS, AR), Acetone (AR) and ammonium metavanadate (NH_4VO_3 , AR) were purchased from Sinopharm Chemical Reagent Co., Ltd. Ammonia solution (25 wt.%), ethanol (AR), methanol (AR), acetic acid (AR), acetonitrile (AR), styrene (CP) and hydrogen peroxide (H_2O_2 , 30 wt.%) were purchased from Nanjing Chemical Reagent Co., Ltd.

Synthesis

A series of vanadium-containing MCM-48 samples with spherical morphology were synthesized as follows. 1.0125 g cetyltrimethylammonium bromide (CTAB) was dissolved in a mixed solvent composed of 69 mL deionized water, 6.3 mL concentrated ammonia solution (25 wt.%) and 32.4 mL ethanol. The pH value of the solution is about 11.0. Then, 10 mL aqueous solution containing desired amount of NH_4VO_3 and 2.1 mL tetraethylorthosilicate (TEOS, 0.0093 mol) were slowly added into the above template solution under stirring. After being stirred for another 2 h, the resulting gel was transferred into Teflon-lined stainless steel autoclaves and kept at 100 °C for 24 h. The sample obtained was washed with deionized water and ethanol for three times, and then dried at room temperature. The as-synthesized product was calcinated at 550 °C in a flow of air for 6 h to remove the template. The obtained samples are denoted as $x\text{V-MCM-48}$, where x is 100 times of the calculated molar ratio of V/Si used in the synthesis gel.

For comparison, V-MCM-48-M (irregular morphology) and V-MCM-48-I (prepared by impregnation) were synthesized referred to the reported literatures¹⁷ and³⁵, respectively.

Characterization

The XRD patterns of the samples were collected with a diffractometer (RigakuD/Max-RAX) equipped with a rotating anode and Cu K α radiation ($\lambda=0.154178$ nm).

N₂ adsorption/desorption isotherms were measured on a Micromeritics ASAP-2020 analyzer at 77 K. Before the measurements, calcined samples were degassed in vacuum at 300 °C for 5 h. Surface areas were calculated using the BET equation and pore size distributions were obtained by the Barrett-Joyner-Halenda (BJH) method using desorption branch data.

High-resolution transmission electron microscopy (HRTEM) images were recorded on a JEM-2010 EX microscope operated at an accelerating voltage of 200 kV. The samples were crushed in A.R. grade ethanol and the resulting suspension was allowed to dry on carbon film supported on copper grids.

Field emission scanning electron microscope (FE-SEM) was performed on a Hitachi S4800 Field Emission Scanning Electron Microscopy.

The vanadium content in the samples was determined using a Jarrell-Ash 1100 Inductively Coupling Plasma emission spectrometer. The samples were completely dissolved in hydrofluoric acid before analysis.

Diffuse reflectance UV-vis spectra were recorded by a Perkin-Elmer Lambda 35 spectrophotometer in the range of 200-800 nm with BaSO₄ as reference.

The X-ray photoelectron spectra (XPS) were conducted on PHI 5000 Versa Probe X-ray

photoelectron spectrometer equipped with Al K_{α} radiation (1486.6 eV). The C1s peak at 284.6 eV was used as the reference for binding energies.

Magic angle spinning nuclear magnetic resonance (MAS-NMR) spectra were collected at Larmor frequency of 105.181 MHz and magnetic field strength of 9.4 T using a 4.0 mm MAS probe with spinning at 14 kHz on a Bruker Avance III spectrometer.

Electron spin-resonance spectroscopy (ESR) spectra were recorded on a Bruker EMX-10/12 ESR spectrometer with X-band at 110 K.

Catalyst test

The catalytic testing was carried out in a two-necked flask placed in a water bath. Typically, 0.1 g catalyst, 20 mL solvent and a desired amount of styrene were mixed. When the temperature reached 30-70 °C, a given amount of H₂O₂ was added dropwise into the reaction mixture under stirring. After reaction for 2-12 h, the catalyst was separated by centrifugation. The product distribution was analyzed by a SP-6890 gas chromatograph (Lunan Ruihong Chemical Instrument Co., Ltd. China) equipped with a 0.32 mm×30 m SE-54 capillary column and a flame ionization detector (FID). The content of each component was calculated by a revised area normalization method.

3. Results and discussion

3.1 Mesostructure

The small-angle XRD patterns of the calcined V-MCM-48 samples with different vanadium content are shown in Fig. 1. The sharp (211) reflection peak at $2\theta \approx 2.4^\circ$ demonstrates the characteristic of a typical mesoporous structure. Other three weak peaks confirmed the presence of highly ordered 3D cubic $Ia\bar{3}d$ mesophase, which are indexed to the (220), (420) and (332) reflections.^{36, 37} Therefore, the results indicate that the 3D

-

cubic *Ia3d* mesostructure was retained for the catalysts modified with vanadium. Moreover, the reflections of 8V-MCM-48 sample become broad and weak, indicating that the over-doping (molar ratio used in the synthesis gel of $V/Si > 0.06$) of vanadium species result in the decrease of the order degree of cubic mesostructure. In particular, no characteristic peaks of vanadium oxides were found in high-angle XRD patterns (figures not given), suggesting that the vanadium species should be incorporated into the framework of MCM-41 or disperse highly on the wall.^{25, 38}

The TEM image of 4V-MCM-48 is depicted in Fig. 2a. A well-ordered mesostructure is clearly visualized and the pore size is found to be in the range of 2.3-2.5 nm, which is in good agreement with the result calculated from the BJH model using desorption data (Fig. 3b). A well-resolved cubic diffraction pattern is observed in FT pattern (Fig. 2b), which demonstrates the regular three-dimensional pore structure of V-MCM-48 sample.^{10, 17, 37} These observations indicate that the moderate incorporation of vanadium atoms influence barely the cubic mesostructure of MCM-48.

Fig. 3 shows the N₂ adsorption-desorption isotherms and pore size distributions of all the samples. The typical IV type isotherms (Fig.3a) are the characteristic of mesoporous solids.³⁹ Due to the capillary condensations of nitrogen, the steep increases of absorption volume in the P/P_0 range of 0.25-0.35 represent the highly ordered mesostructure of the materials and very narrow pore size distributions, which are evident in Fig.3b.^{10, 35, 37} Some structural parameters of the samples are listed in Table 1. As illustrated in Table 1, no apparent changes are observed for the most probable pore diameter of all the samples, which suggests that the incorporation of vanadium has little influence on the pore size distribution. The BET surface area and the total pore volume decrease with the increase

of vanadium content, which maybe results from the decreased order degree of mesostructure caused by high amount of vanadium doping, respectively. The total pore volumes decrease with the increase of vanadium content, which suggests the formation of extra-framework vanadium species.

The recorded data as well as the analyzed results above demonstrate that we offer a convenient strategy to produce highly ordered cubic mesoporous materials incorporated with moderate amount of vanadium. Although the overload of vanadium does not influence on the pore size distribution, it will evitably cause the distortion of mesostructure of materials.

3.2 Morphology

The representative SEM and TEM images of samples are shown in Fig. 4. As shown in Fig. 4a, the regularly and homogeneously dispersed spherical particles of 4V-MCM-48 sample are clearly visible. The TEM image (Fig. 4b) confirms the spherical morphology with uniform particle size of about 0.5 μm . For 8V-MCM-48 sample (Fig. 4c), although there are a few particles with other morphologies, the spherical particles are dominant. In addition, Fig. 4d shows the irregular sample synthesized as previously reported.¹⁷

According to Stöber process,^{40, 41} small particles of silicate are initiated, which aggregate gradually to form a spherical morphology. In this study, we suggested the formation of spherical V-MCM-48 follow the similar procedures. As shown in scheme 1, the micelles are produced from the template solution (step I). Both TEOS and vanadium source hydrolyze to form disordered clusters(step II), which grow into large and packed particles(step III). To minimize the surface free energy,^{10, 13} the particles of large size will further aggregate into a spherical form.

Note that the pH value is ca.11 and the $-\log(V/\text{mol}\cdot\text{L}^{-1})$ values decrease from 2.6 to 2.1 with the increasing amount of vanadium. According to the occurrence of various vanadate and polyvanadate species as a function of pH and total concentration of vanadium depicted in Ref. 42 (Page 984), the vanadium species mainly exist as two species, HVO_4^{2-} and $\text{V}_2\text{O}_7^{4-}$.⁴² And the proportion of $\text{V}_2\text{O}_7^{4-}$ should increase with the increasing amount of vanadium considering the equation $2[\text{HVO}_4^{2-}]^{2-} \rightleftharpoons [\text{V}_2\text{O}_7]^{4-} + \text{H}_2\text{O}$.⁴² Therefore, HVO_4^{2-} is reduced to V (IV) by ethanol and hydrolyzes simultaneously with TEOS to form V-MCM-48 clusters with tetrahedral V^{4+} ions in the framework (step II). Meanwhile, $\text{V}_2\text{O}_7^{4-}$ species with larger ionic diameters either stay in the solution which results in materials of much lower vanadium content than expected or serve as the source of V^{5+} species in MCM-48.

Therefore, in the cases of lower concentration of $\text{V}_2\text{O}_7^{4-}$ in the solution, the MCM-48 clusters may favor the growth into a spherical form. By contrast, at higher concentration of $\text{V}_2\text{O}_7^{4-}$, the MCM-48 clusters will become the irregular particles due to the electrostatic repulsion.

3.3 The states of vanadium species

UV-vis

As shown in Fig. 5, the UV-vis spectrum of pure MCM-48 support exhibits little absorption in the range of 200-700 nm.¹² All the V-MCM-48 samples show two distinct absorption bands, in which an intense broad band between 220 nm and 320 nm centered at 260 nm is assigned to low-energy charge-transfer transitions between tetrahedral oxygen ligands and central V^{4+} ion present in the framework, and the intense band centered at 370 nm is attributed to the isolated V^{5+} species with tetrahedral structure that

incorporated on the silicate surface of MCM-48. UV-Vis absorption band at ca. 450 nm of octahedral structure of extra-framework V^{5+} may be covered by the tails of absorption lines decreasing up to ca. 550 nm.^{20, 43} The band of bulk V_2O_5 crystallites (ca. 450 to 480 nm) is not observed for all samples,^{17, 18} which accords well with XRD results.

It is found that the intensity of the two absorbance bands increases with the vanadium content, which is more evident for the bands centered at 370 nm indicating the presence of more V^{5+} species dispersed on the surface.

XPS

The XPS spectra of obtained materials are given in Fig. 6. The broad asymmetrical $V2p_{3/2}$ spectra can be de-convoluted into two components at about 516.2 eV and 517.4 eV, which are assigned to V^{4+} and V^{5+} , respectively.^{32, 44} The peak area at 516.2 eV is found to be larger than that of 517.4 eV, indicating that the V^{4+} species is dominant in V-MCM-48 samples. Moreover, the ratio of peak areas at 517.4 eV relative to 516.2 eV increases with the amount of vanadium species, demonstrating more V^{5+} species disperse on the surface in the samples. These findings further support the conclusion obtained from UV-vis spectroscopy.

Furthermore, by inspection of Table 1, it can be seen that the bulk vanadium contents in 4V-MCM-48, 6V-MCM-48 and 8V-MCM-48 samples determined by ICP are much higher than those of surface vanadium content obtained from XPS. This observation indicates that most of vanadium species are incorporated into the framework of MCM-48.

^{51}V MAS-NMR

^{51}V MAS-NMR spectra of 4V-MCM-48, 6V-MCM-48 and 8V-MCM-48 samples were also recorded. As depicted in Fig. 7, the relatively weak signals at -585 ppm are observed

in 6V-MCM-48 and 8V-MCM-48 samples, which are ascribed to the characteristic of V^{5+} in tetrahedral environment.^{17, 25, 38, 45} Moreover, the signal intensity becomes weaker with the decrease of the amount of vanadium, and no distinguished signal observed for 4V-MCM-48 sample possibly due to its weak signal-to-noise (S/N) ratio. This observation indicates that more existence of V^{5+} species in the sample with the increasing amount of vanadium, which is consistent with the results of UV-vis and XPS measurements. Meanwhile, there are no characteristic peaks around -300 ppm observed in all samples suggesting the absence of bulk V_2O_5 crystallites.^{17, 38}

ESR

To further evaluate the states of vanadium, the ESR spectra of samples were acquired. As shown in Fig. 8, all the samples exhibit an axially symmetrical signal of V^{4+} which results from the d^1 electron interaction with nuclear spin $I_n=7/2$ of ^{51}V (natural abundance 99.8%).⁴⁵ The spin Hamiltonian parameters A tensor and g tensor were determined as $g_{||}= 1.94$, $A_{||}= 197$ G, $g_{\perp}=1.98$, and $A_{\perp}= 64$ G, which is typified as tetrahedral V^{4+} species.²⁵ In addition, the ESR signal intensity of the calcined V-MCM-48 samples increases linearly with the increasing vanadium content. No observation of spin-spin interactions among V^{4+} ions indicates that V^{4+} should be highly dispersed in the silicate matrix.^{25, 45, 46}

To summarize the characterization results from UV-vis, XPS, ^{51}V MAS-NMR and ESR, we find that there are two types of vanadium species existing in spherical V-MCM-48 materials that we produced, i.e. the tetrahedral V^{4+} ions in the framework, and the V^{5+} species dispersed on the surface, as illustrated in Fig. 9.

3.4 Catalytic activity

Catalytic performance of vanadium-containing MCM-48

Active sites. Table 2 summarizes the catalytic activity of produced materials in styrene oxidation to benzaldehyde. Pure MCM-48 exhibited no catalytic activity due to the absence of active sites.^{12, 13} Crystalline V_2O_5 exhibits improved catalytic activity, which indicates that V^{5+} species act as active sites. Accordingly, V-MCM-48-I prepared by impregnation method possesses a larger turnover number (TON) value compared with crystalline V_2O_5 which should attribute to the dispersion of V^{5+} species. Notably, the degree of dispersion of V^{5+} species is further improved for V-MCM-48 prepared by DHT method,⁴⁷ which results in remarkably higher catalytic activity and TON value.

Reaction mechanism. Considering that the V^{5+} acts as active sites, we propose that the oxidation of styrene over vanadium-doping MCM-48 catalyst should involve the following reaction processes, similar to that over La-MCM-48.⁴⁸ Three main reaction steps should be involved, as shown in Scheme 2: (1) V^{5+} ($(SiO)_3V=O$) and V^{4+} ($(SiO)_3V-OH$) species on the surface of materials react with H_2O_2 to form V-superoxo ($VOOH$) species; (2) Styrene molecules react with V-superoxo species to form styrene epoxide; (3) Styrene epoxide is further oxidized by H_2O_2 to obtain benzaldehyde.^{27, 48}

Effect of spherical morphology

We know that the performance of catalyst is often related to the amount of active sites, morphology and structural parameters of the support. As listed in Table 2, it is found that the catalytic activities of V-MCM-48 samples firstly increase and then decrease with the increasing content of vanadium. And, the respective structural parameters of all samples, such as total pore volume and BET specific surface area, are observed to be decreased with increased vanadium content (Table 1). Therefore, the unexpected dependence of

catalytic activity of materials on the vanadium content suggests that morphology plays an essential role for the remarkable catalytic performance of materials. Specifically, for the 2V- and 4V-MCM-48 samples with similar spherical morphology, their catalytic activities are highly related to the amount of vanadium. By comparison, despite its improved vanadium content, 8V-MCM-48 sample of irregular forms shows a dramatic decrease of catalytic activity. In fact, comparing with V-MCM-48-M sample with irregular morphology, spherical 4V-MCM-48 which contains the same vanadium content exhibits markedly improved catalytic activity. These observations can be explained by the fact that the regularly spherical morphology can speed up the mass transport involved in catalytic reaction in heterogeneous catalysis thus contribute to an improved catalytic performance of materials.¹¹⁻¹⁴ Next, we explored the optimization of reaction condition on the basis of 4V-MCM-48 catalyst.

Optimization of reaction condition

Molar ratio of H₂O₂/styrene. In the range of molar ratio of H₂O₂/styrene from 0.5 to 2, the styrene conversion is observed to be increased significantly from 23% to 83%. At higher molar ratio of H₂O₂/styrene (>2), the styrene conversion decreases. This observation accords well with the reaction mechanism as totally two H₂O₂ molecules are involved in the reaction. The selectivity to benzaldehyde is observed to be in the range of 89.6% - 97.7% at different molar ratio of H₂O₂/styrene. Therefore, we choose the molar ratio of H₂O₂/styrene equal to 2 for the current study.

Reaction temperature. We find that the styrene conversion first increases with temperature from 30 to 50 °C and then decreases slightly at higher temperature (70 °C), which should involve the rapid decomposition of hydrogen peroxide. Meanwhile, the

selectivity to benzaldehyde decreases at higher temperature possibly due to the deep oxidation of products. The highest yield of benzaldehyde is observed at 50 °C.

Reaction time. As observed in Fig.10, the styrene conversion increases from 40.7% to 52.1% in a reaction time ranging from 2-12 h. Prolonged reaction time makes the styrene conversion almost unchanged with a slight decrease of selectivity to benzaldehyde. 12 h is the optimal reaction time.

Solvents. For most of liquid-phase reactions, solvent is an essential factor since it affects the reaction kinetics as well as the product selectivity. Usually, the aprotic solvent is more effective in the catalytic oxidation of aromatics than the protic solvent.⁴⁸ The solvent of higher polarity will increase the substrate concentration which favors the catalytic reaction.⁴⁹ As listed in Table 3, the lower styrene conversion is observed in methanol and acetic acid (protic) than in acetone and acetonitrile (aprotic). Since acetonitrile possesses a higher polarity than that of acetone, the styrene conversion in acetonitrile is found to be higher. The acidity of acetic acid is favorable to the open-ring (C-O-C) reaction in styrene epoxide as mentioned in the second step of reaction mechanism, which results in a higher selectivity to benzaldehyde. On the contrary, methanol is involved in the third step of reaction mechanism which makes the selectivity to benzaldehyde much lower.⁴⁸

Stability. From the test of catalyst stability, we found that the conversion of styrene decreased from 39.2% (fresh catalyst), 28.5% (first recycle) to 12.3% (second recycle) owing to the leaching of a small amount of vanadium ions and the selectivity to benzaldehyde is in the range of 90.2 to 95.5%. The result indicated that 4V-MCM-48 is more resistant to the leaching of vanadium ions because of the vanadium ions incorporated in the silicate framework, which is necessary for the stability of

vanadium-containing silicate catalyst.

From above experimental results, 4V-MCM-48 catalyst exhibited the best activity with 83.0% conversion of styrene and 90.5% selectivity to benzaldehyde under the optimized reaction conditions of the 2:1 molar ratio of H₂O₂/ styrene with acetonitrile as solvent at 50 °C for 12 h.

Conclusions

We have successfully synthesized a series of V-MCM-48 samples with different content of vanadium, which exhibit the spherical morphology and highly ordered 3D-cubic pore structures, by one-step hydrothermal method. The sphere particles are formed following Stöber process, in which small particles with 3D-cubic mesoporous structure start to form after the hydrolysis of silicon and vanadium sources on the pre-aggregated micelles of template, and then grow into spherical morphology.

The characterization results reveals the existence of two types of vanadium species including the tetrahedral V⁴⁺ in the framework and surface-dispersed V⁵⁺ in the produced materials. We identify that V⁵⁺ species on the surface and/or produced from the oxidation of some V⁴⁺ in the framework by H₂O₂ act as active sites in the catalytic conversion of styrene to benzaldehyde. Although the catalytic performance of materials is closely related to the number of active vanadium species, the spherical morphology plays dominant role due to the speeding up of mass transport. Under the optimal reaction condition, the conversion of styrene and the selectivity to benzaldehyde are 83.0% and 90.5%, respectively. Taken all, we offer a facile method to synthesize spherical V-MCM-48 with excellent catalytic activity.

Acknowledgments

The authors acknowledge the financial support of the National Natural Science Foundations of China (21276125, 20876077, 21476108), the Major Projects of the Natural Science Foundation for the Higher Education Institutions of Jiangsu Province (10KJA530015), the Program for Scientific Innovation Research of College Graduates in Jiangsu Province (CXZZ13_0443), the Key Program of National Natural Science Foundation of China (No. 21136005) and the Project of Priority Academic Program Development of Jiangsu Higher Education Institutions (PAPD).

Notes and references

1. C. T. Kresge, M. E. Leonowicz, W. J. Roth, J. C. Vartuli and J. S. Beck, *Nature*, 1992, **359**, 710-712.
2. M. Egi, K. Sugiyama, M. Saneto, R. Hanada, K. Kato and S. Akai, *Angew. Chem. Int. Edit.*, 2013, **52**, 3654-3658.
3. S. Dib, M. Boufatit, S. Chelouaou, F. Sadi-Hassaine, J. Croissant, J. Long, L. Raehm, C. Charnay and J. O. Durand, *Rsc Adv.*, 2014, **4**, 24838-24841.
4. Y. Zhou, W. G. Lin, M. M. Wan, J. Yang and J. H. Zhu, *J. Mater. Chem.*, 2012, **22**, 23633-23641.
5. F. Muharnmad, M. Guo, W. Qi, F. Sun, A. Wang, Y. Guo and G. Zhu, *J. Am. Chem. Soc.*, 2011, **133**, 8778-8781.
6. S. H. Cheng, C. H. Lee, C. S. Yang, F. G. Tseng, C. Y. Mou and L. W. Lo, *J. Mater. Chem.*, 2009, **19**, 1252.
7. S. Gomez, L. J. Garces, J. Villegas, R. Ghosh, O. Giraldo and S. L. Suib, *J. Catal.*, 2005, **233**, 478-478.
8. T. W. Kim, F. Kleitz, B. Paul and R. Ryoo, *J. Am. Chem. Soc.*, 2005, **127**, 7601-7610.
9. T. Suteewong, H. Sai, R. Cohen, S. T. Wang, M. Bradbury, B. Baird, S. M. Gruner and U. Wiesner, *J. Am. Chem. Soc.*, 2011, **133**, 172-175.
10. T. W. Kim, P. W. Chung and V. S. Y. Lin, *Chem. Mater.*, 2010, **22**, 5093-5104.
11. T. M. Suzuki, T. Nakamura, K. Fukumoto, M. Yamamoto, Y. Akimoto, Y. Akimoto and K. Yano, *J. Mol. Catal. A-Chem.*, 2008, **280**, 224-232.
12. A. I. Carrillo, E. Serrano, R. Luque and J. Garcia-Martinez, *Appl. Catal. A-Gen.*, 2013, **453**, 383-390.
13. Y. Chen, X. Shi, B. Han, H. Qin, Z. Li, Y. Lu, J. Wang and Y. Kong, *J. Nanosci. Nanotechnol.*, 2012, **12**, 7239-7249.
14. G. C. Bond, *Heterogeneous Catalysis Principles and Applications[M]*, 1982.
15. Z. Yang, Y. Lu and Z. Yang, *Chem. Commun.*, 2009, 2270-2277.
16. C. C. Liu, X. M. Wang, S. Lee, L. D. Pfefferle and G. L. Haller, *Micropor. Mesopor. Mater.*, 2012, **147**, 242-251.
17. P. Selvam and S. E. Dapurkar, *Appl. Catal. A-Gen.*, 2004, **276**, 257-265.
18. S. Q. Hu, D. P. Liu, L. S. Li, A. Borgna and Y. H. Yang, *Catal. Lett.*, 2009, **129**, 478-485.
19. J. Strunk, W. C. Vining and A. T. Bell, *J. Phys. Chem. C*, 2010, **114**, 16937-16945.
20. Y. Kong, R. Zhang, X. J. Xu, Z. L. Wang and J. Wang, *Chinese J. Inorg. Chem.*, 2008, **24**, 1124-1127.
21. C. Wu, Y. Kong, F. Gao, Y. Wu, Y. N. Lu, J. Wang and L. Dong, *Micropor. Mesopor. Mater.*, 2008, **113**, 163-170.
22. Y. Wu, Y. Zhang, J. Cheng, Z. Li, H. Wang, Q. Sun, B. Han and Y. Kong, *Micropor. Mesopor. Mater.*, 2012, **162**, 51-59.
23. F. T. Kuo, S. Y. Chen, T. H. Lin, J. F. Lee and S. Cheng, *Rsc Adv.*, 2013, **3**, 12604-12610.
24. J. Sun, Q. Kan, Z. Li, G. Yu, H. Liu, X. Yang, Q. Huo and J. Guan, *Rsc Adv.*, 2014, **4**, 2310-2317.
25. F. Gao, Y. H. Zhang, H. Q. Wan, Y. Kong, X. C. Wu, L. Dong, B. Q. Li and Y. Chen, *Micropor. Mesopor. Mater.*, 2008, **110**, 508-516.
26. M. A. Betiha, H. M. A. Hassan, A. M. Al-Sabagh, A. E. R. S. Khder and E. A. Ahmed, *J. Mater. Chem.*, 2012, **22**, 17551-17559.
27. M. Piumetti, M. Armandi, E. Garrone and B. Bonelli, *Micropor. Mesopor. Mater.*, 2012, **164**, 111-119.
28. S. Samanta, S. Das, P. K. Samanta, S. Dutta and P. Biswas, *Rsc Adv.*, 2013, **3**, 19455-19466.
29. G. Zhang, J. Long, X. Wang, Z. Zhang, W. Dai, P. Liu, Z. Li, L. Wu and X. Fu, *Langmuir*, 2010, **26**, 1362-1371.
30. L. L. Lou, S. Jiang, K. Yu, Z. Gu, R. Ji, Y. Dong and S. Liu, *Micropor. Mesopor. Mater.*, 2011, **142**, 214-220.
31. C. He, J. Li, P. Li, J. Cheng, Z. Hao and Z. P. Xu, *Appl. Catal. B-Environ.*, 2010, **96**, 466-475.
32. B. Guo, L. F. Zhu, X. K. Hu, Q. Zhang, D. M. Tong, G. Y. Li and C. W. Hu, *Catal. Sci. & Technol.*, 2011, **1**, 1060-1067.
33. L. Y. Hu, B. Yue, X. Y. Chen and H. Y. He, *Catal. Commun.*, 2014, **43**, 179-183.

34. Y. Wu, Y. J. Zhang, J. Cheng, Z. Li, H. Q. Wang, Q. L. Sun, B. Han and Y. Kong, *Micropor. Mesopor. Mater.*, 2012, **162**, 51-59.
35. A. Benhamou, M. Baudu, Z. Derriche and J. P. Basly, *J. Hazard. Mater.*, 2009, **171**, 1001-1008.
36. A. Sayari, *J. Am. Chem. Soc.*, 2000, **122**, 6504-6505.
37. W. Zhao, Q. Li, L. Wang, J. Chu, J. Qu, S. Li and T. Qi, *Langmuir*, 2010, **26**, 6982-6988.
38. M. Piumetti, B. Bonelli, M. Armandi, L. Gaberova, S. Casale, P. Massiani and E. Garrone, *Micropor. Mesopor. Mater.*, 2010, **133**, 36-44.
39. W. Zhao, Q. Z. Li, L. N. Wang, J. L. Chu, J. K. Qu, S. H. Li and T. Qi, *Langmuir*, 2010, **26**, 6982-6988.
40. K. T. Lee, A. N. Sathyagal and A. V. McCormick, *Colloid. Surf. A*, 1998, **144**, 115-125.
41. K. Schumacher, P. I. Ravikovitch, A. Du Chesne, A. V. Neimark and K. K. Unger, *Langmuir*, 2000, **16**, 4648-4654.
42. N. N. Greenwood, *Chemistry of the Elements [M]*, 1996.
43. C. Subrahmanyam, B. Louis, B. Viswanathan, A. Renken and T. K. Varadarajan, *Appl. Catal. A-Gen.*, 2005, **282**, 67-71.
44. C. T. Wang, M. T. Chen and D. L. Lai, *Appl. Surf. Sci.*, 2011, **257**, 5109-5114.
45. M. Chatterjee, T. Iwasaki, H. Hayashi, Y. Onodera, T. Ebina and T. Nagase, *Chem. Mater.*, 1999, **11**, 1368-1375.
46. A. Held, J. Kowalska-Kus and K. Nowinska, *Catal. Commun.*, 2012, **17**, 108-113.
47. M. Piumetti, B. Bonelli, P. Massiani, S. Dzwigaj, I. Rossetti, S. Casale, M. Armandi, C. Thomas and E. Garrone, *Catal. Today*, 2012, **179**, 140-148.
48. W. C. Zhan, Y. L. Guo, Y. Q. Wang, X. H. Liu, Y. Guo, Y. S. Wang, Z. G. Zhang and G. Z. Lu, *J. Phys. Chem. B*, 2007, **111**, 12103-12110.
49. D. Chen, N. Li, P. Sun and Y. Kong, *Chinese J. Catal.*, 2009, **30**, 643-648.

Table 1 The structural properties of V-MCM-48 samples

Sample	V/Si molar ratio ^a /%	V/Si molar ratio ^b /%	$S_{\text{BET}}^{\text{c}}$ ($\text{m}^2 \cdot \text{g}^{-1}$)	D_{211} (nm)	a_0^{d} (nm)	D_{p}^{e} (nm)	W_{t}^{f} (nm)	Total pore volume ($\text{cm}^3 \cdot \text{g}^{-1}$)
2V-MCM-48	0.71	/ ^g	1090	3.56	8.73	2.39	1.63	0.73
4V-MCM-48	1.29	0.41	969	3.59	8.80	2.40	1.65	0.72
6V-MCM-48	1.95	0.59	944	3.59	8.80	2.42	1.64	0.65
8V-MCM-48	2.88	1.04	788	3.56	8.73	2.39	1.63	0.56

^a Calculated from ICP data. ^b Obtained from XPS data. ^c BET surface area. ^d Unit cell parameter (a_0) calculated using $a_0 = d_{211} \sqrt{6}$. ^e Pore sizes obtained from BJH analysis of desorption data. ^f Wall thickness = $(a_0/3.0919) - [(pore\ size)/2]$. ^g Not available.

Table 2 Catalytic performance of vanadium-containing catalysts

Catalyst	V/Si ^a (%)	Conversion (%)	TON ^b	Selectivity (%)			
				BZ ^c	PhA ^d	SE ^e	BA ^f
Pure MCM-48	0.00	-	-	-	-	-	-
2V-MCM-48	0.71	22.0	224	95.2	1.7	1.1	1.0
4V-MCM-48	1.29	39.2	257	95.5	1.8	1.2	-
6V-MCM-48	1.95	44.1	231	94.5	1.8	1.1	1.2
8V-MCM-48	2.88	40.1	166	94.3	1.7	1.1	1.0
V-MCM-48-M	1.35	25.6	166	91.0	1.0	2.4	1.0
4V-MCM-48-I	1.22	10.2	98	91.7	1.3	1.9	1.1
8V-MCM-48-I	2.98	18.4	70	90.3	1.2	2.1	1.0
V ₂ O ₅	-	11.1	21	91.3	1.6	1.8	1.2

^a The molar ratio of V/Si determined by ICP, ^b Turnover number (TON), ^c Benzaldehyde, ^d Phenyl acetaldehyde, ^e Styrene epoxide, ^f Benzoic acid.

Reaction condition: temperature 30 °C, styrene 2.2 mL, H₂O₂ 2 mL, catalyst 0.1 mg, reaction time 12 h and acetonitrile 20 mL.

Table 3 Effects of solvents on the catalytic performance

Solvent	Conversion (%)	Selectivity (%)			
		BZ	PhA	SE	BA
Methanol	22.1	37.3	0.8	7.0	23.6
Acetic acid	39.1	93.8	0.9	1.0	1.9
Acetone	42.9	84.5	0.94	2.3	0.9
Acetonitrile	52.1	96.5	0.8	1.1	0.6

Reaction condition: styrene 2.2 mL, H₂O₂ 2 mL, temperature 50 °C, catalyst 0.1 mg, reaction time 12 h and solvent 20 mL.

Figure captions

Fig.1 XRD patterns of the calcined V-MCM-48 samples

Fig.2 Representative TEM and SAED images of calcined 4V-MCM-48 samples

Fig.3 N₂ adsorption-desorption isotherms (a) and pore diameter distributions (b) of calcined V-MCM-48 samples

Fig.4 SEM images of calcined 4V-MCM-48 (a), 8V-MCM-48 (c) and V-MCM-48-M (d) samples and TEM image of calcined 4V-MCM-48 (b)

Fig.5 UV-vis spectra of calcined V-MCM-48 and pure MCM-48 samples

Fig.6 XPS V 2p_{3/2} spectra of calcined V-MCM-48 samples

Fig.7 ⁵¹V MAS-NMR spectra of calcined V-MCM-48 samples

Fig.8 ESR spectra of calcined V-MCM-48 samples

Fig.9 Proposed structure of V⁴⁺ (a) in silicate framework and V⁵⁺ (b) on the surface

Fig.10 Effects of reaction time on conversion of styrene and selectivity to benzaldehyde. Reaction conditions: styrene 2.2 mL, H₂O₂ 2 mL, catalyst 0.1 mg, acetonitrile 20 mL and temperature 50 °C.

Scheme 1 Proposed formation mechanism of spherical V-MCM-48 based on Stöber process

Scheme 2 Proposed reaction mechanism for the oxidation of styrene over V-MCM-48 catalyst

Fig.1

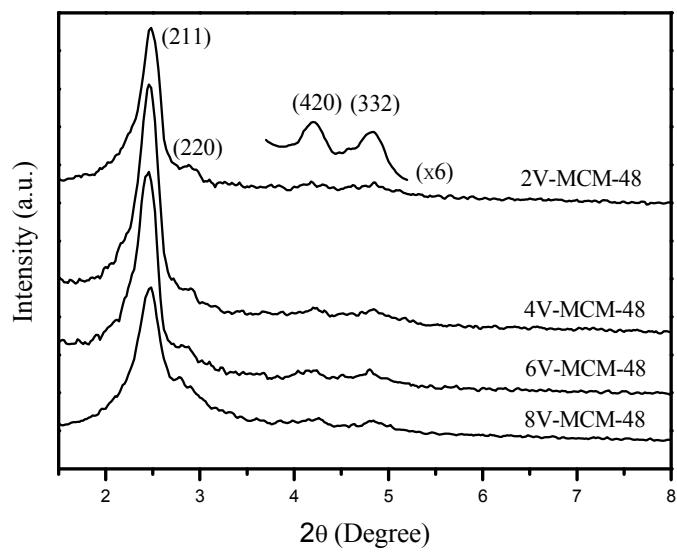


Fig.2

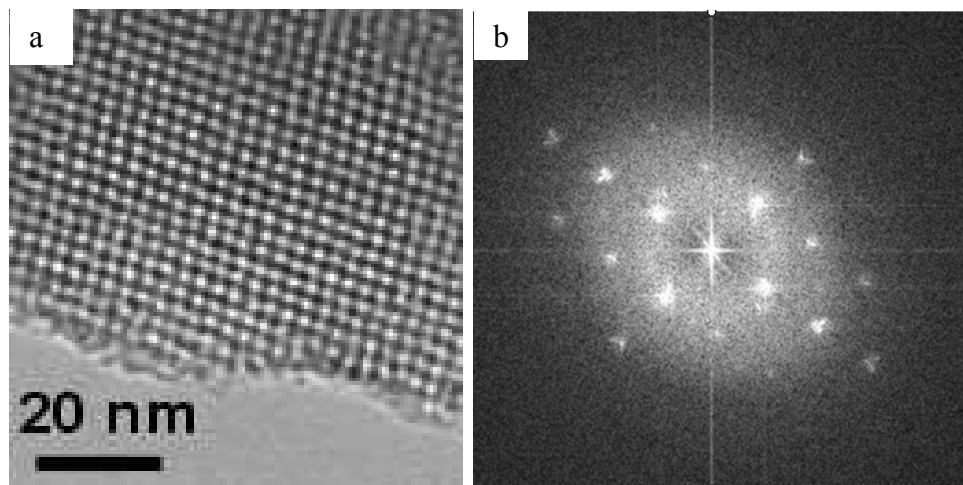


Fig.3

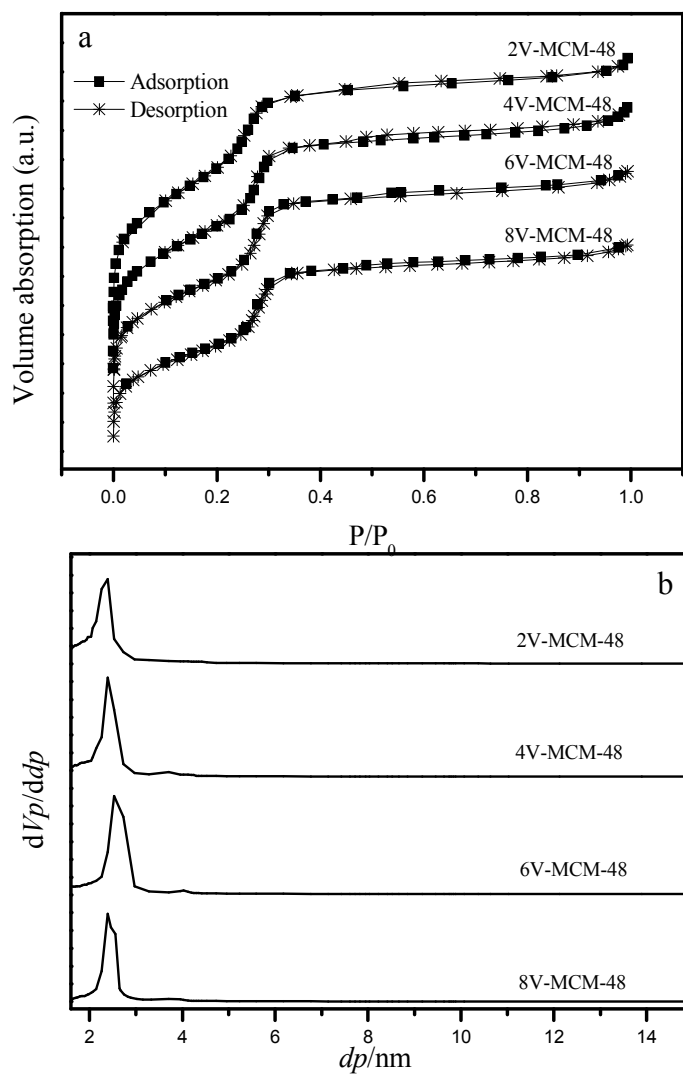


Fig.4

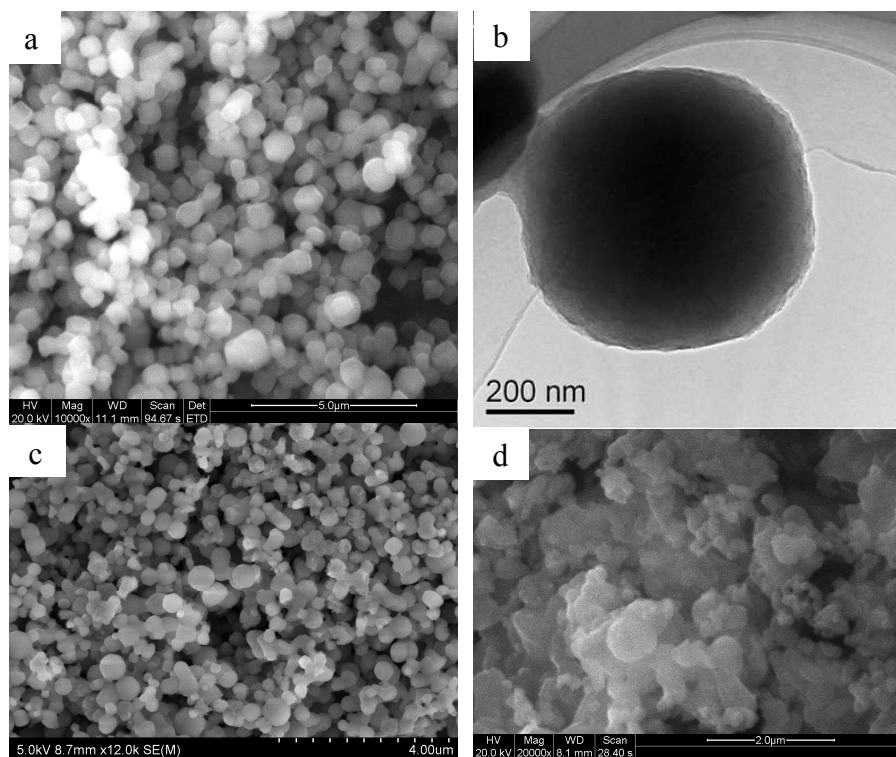


Fig.5

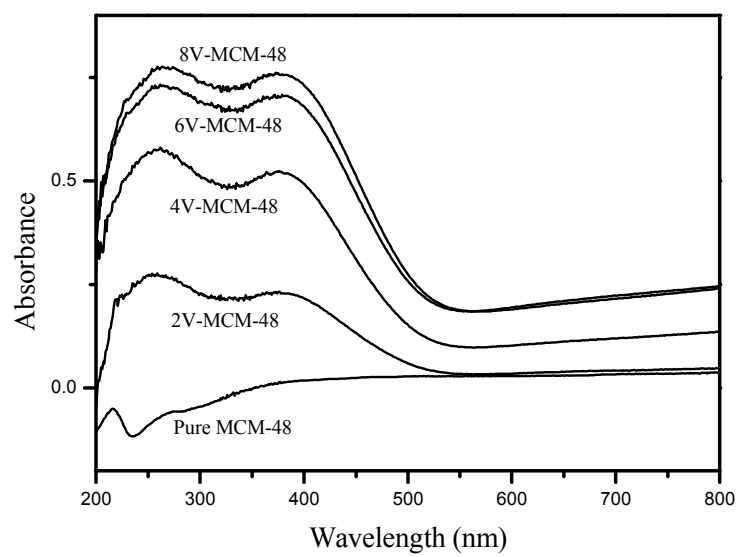


Fig.6

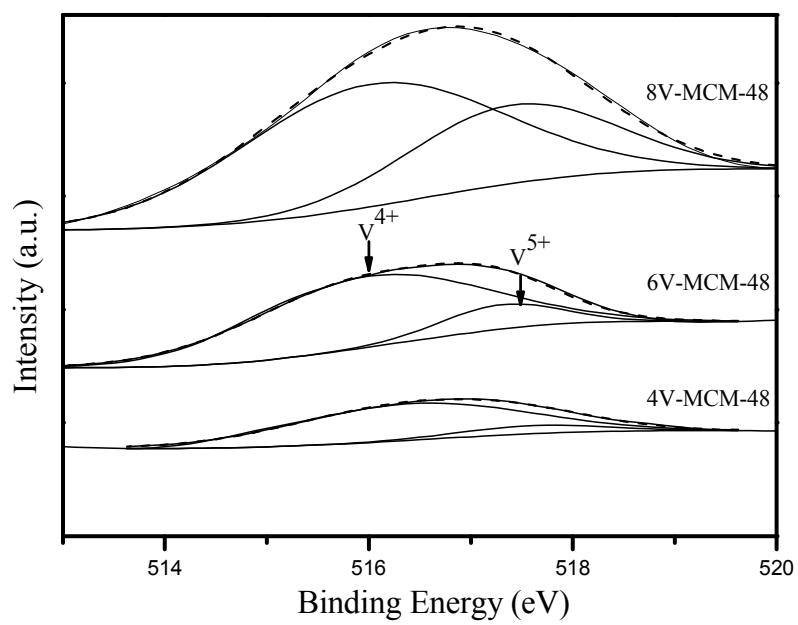


Fig.7

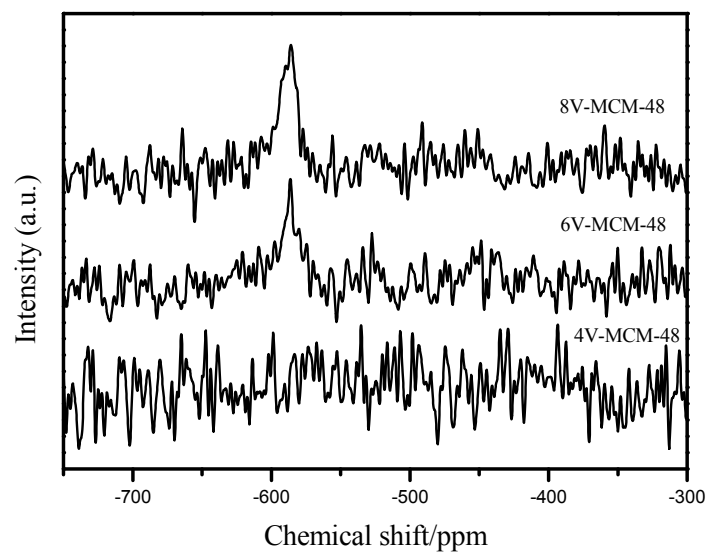


Fig.8

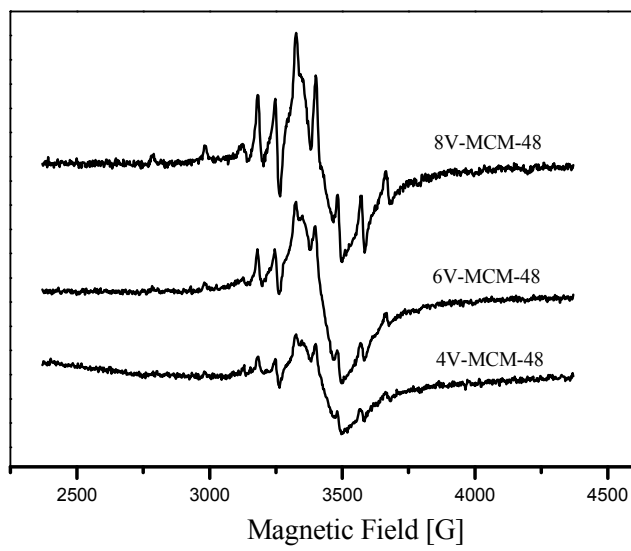
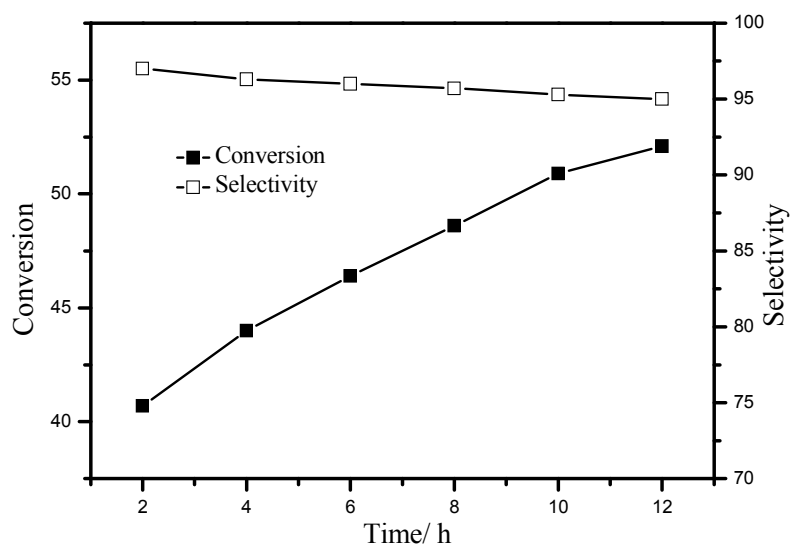
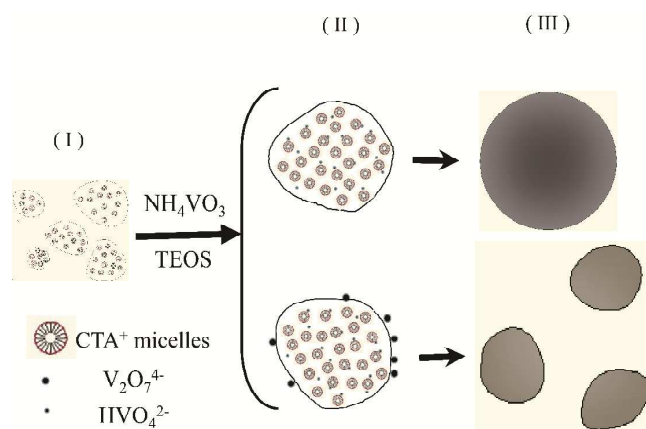
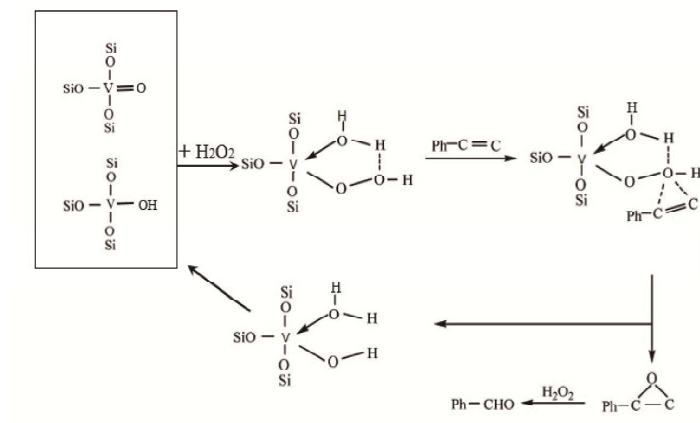


Fig.10

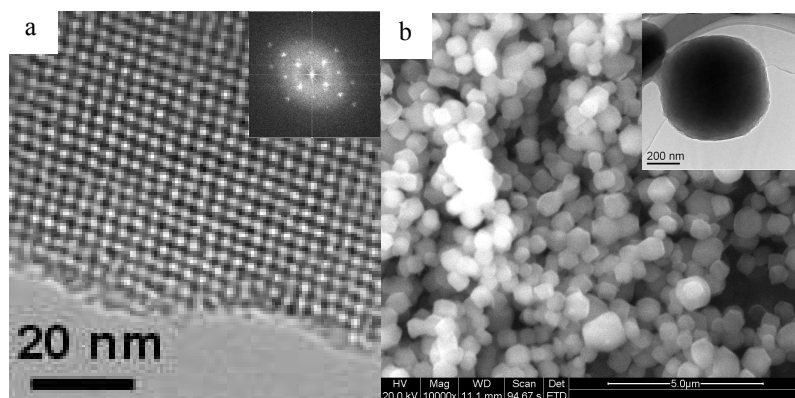




Scheme 1 The proposed formation mechanism of spherical V-MCM-48 based on Stöber process



Scheme 2 Proposed reaction mechanism for the oxidation of styrene over V-MCM-48 catalyst



High-quality spherical V-MCM-48 catalysts were successfully synthesized and showed higher catalytic activity in selective oxidation of styrene to benzaldehyde.